Hysteretic Vortex-Matching Effects in High-T_c Superconductors with Nanoscale Periodic Pinning Landscapes Fabricated by He Ion-Beam Projection

G. Zechner, F. Jausner, L. T. Haag, and W. Lang*

Faculty of Physics, Electronic Properties of Materials, University of Vienna, Boltzmanngasse 5, A-1090 Wien, Austria

M. Dosmailov, M. A. Bodea, and J. D. Pedarnig

Institute of Applied Physics, Johannes-Kepler-University Linz, Altenbergerstrasse 69, A-4040 Linz, Austria

(Received 20 February 2017; revised manuscript received 22 June 2017; published 21 July 2017)

Square arrays of submicrometer columnar defects in thin $YBa_2Cu_3O_{7-\delta}$ (YBCO) films with spacings down to 300 nm are fabricated by a He ion-beam projection technique. Pronounced peaks in the critical current and corresponding minima in the resistance demonstrate the commensurate arrangement of flux quanta with the artificial pinning landscape, despite the strong intrinsic pinning in epitaxial YBCO films. While these vortex-matching signatures are exactly at the predicted values in field-cooled experiments, they are displaced in zero-field-cooled, magnetic-field-ramped experiments, conserving the equidistance of the matching peaks and minima. These observations reveal an unconventional critical state in a cuprate superconductor with an artificial, periodic pinning array. The long-term stability of such out-of-equilibrium vortex arrangements paves the way for electronic applications employing fluxons.

DOI: 10.1103/PhysRevApplied.8.014021

I. INTRODUCTION

Investigations of magnetic vortices in superconductors interacting with periodic pinning arrays have been motivated by the rich diversity of different physical phenomena that result from the interplay of pinning, elastic, and thermal energies and the influences of the dimensionality, anisotropy, and spatial arrangement of vortices [1–17]. However, the motion of vortices in a superconductor also gives rise to dissipation that is detrimental for most technical applications. Developing efficient strategies to block the mobility of vortices is, therefore, one of the high-priority goals of current applied superconductivity research. Tailored artificial pinning defects offer not only the chance to realize enhanced vortex pinning but also many different ways of flux quanta manipulation, like guided vortex motion [18], vortex ratchets [19,20], and valves—building blocks for fast data manipulation and low-dissipative computer circuits [21,22]. An important prerequisite for such an undertaking is the realization of stable fluxon arrangements in nonequilibrium positions within the artificial pinning landscape, in analogy to the critical state in unpatterned hard superconductors.

To date, primarily metallic superconductors have been used to study regular artificial defects, although cuprate high-T_c superconductors (HTSCs) would offer much more convenient cooling requirements. In HTSCs, however, the anisotropic layered structure, strong thermal fluctuations and the *d*-wave symmetry of the order parameter introduce additional complexity. Also, the typical average distance of intrinsic defects in $YBa_2Cu_3O_{7-\delta}$ (YBCO) films is about 300 nm [23]. Therefore, the common methods for patterning artificial arrays employed for metallic superconductors, typically allowing for micrometer-scale lattices, are of only limited use for HTSC films. Addressing these issues, we report on an elegant method for fabricating periodic artificial pinning landscapes into thin YBCO films and on hysteretic commensurability effects between fluxons and the pinning arrays that demonstrate stable nonequilibrium arrangements of flux quanta.

II. EXPERIMENTAL TECHNIQUES

Thin films of $YBa_2Cu_3O_{7-\delta}$ are grown epitaxially on (100) MgO single-crystal substrates by pulsed-laser deposition using 248-nm KrF-excimer-laser radiation at a fluence of 3.2 J/cm^2 resulting in thicknesses of the films of $t_z = (210 \pm 10)$ nm. The critical temperatures of the as-prepared films are $T_c \sim 90$ K, the transition width $\Delta T_c \sim 1$ K, and the critical current density $j_c \sim 3$ MA/cm^2 at 77 K and zero magnetic field. For the electrical transport measurements, two identical bridges with dimensions of 240×60 μm^2 are patterned by photolithography and wet chemical etching. Contacts are established in a four-probe geometry using sputtered Au pads with a voltage-probe distance of 100 μm.

The pinning landscape in the films is created by masked ion-beam irradiation (MIBS), sketched in Fig. 1(a). It takes advantage of the fact that irradiation of YBCO with He^+

*wolfgang.lang@univie.ac.at

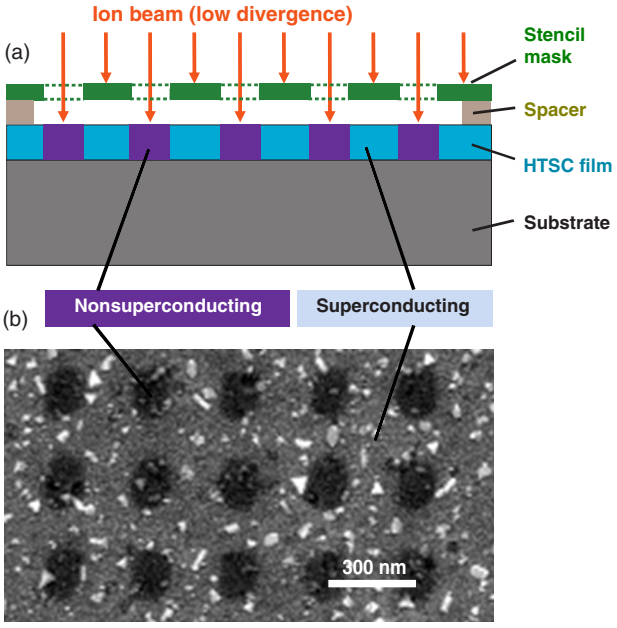

FIG. 1. (a) The principle of MIBS. (b) Scanning-electron-microscopy (secondary-electron-detection) picture of the surface of a thin YBCO film after MIBS with 75-keV He^+ ion irradiation. The dark regions correspond to an array of defect-rich, nonsuperconducting nanocylinders.

ions of moderate energy (75 keV in our experiment) leads to a suppression of the critical temperature T_c. This effect is due to a displacement of mainly the chain oxygen atoms, while the skeleton of the crystalline structure remains intact [24]. A thin Si stencil mask (custom fabricated with *e*-beam lithography by IMS Chips, Germany) is placed on top of the YBCO film and kept at a well-defined distance by a circumferential spacer layer of 1.5-μm-thick photoresist. Under this procedure, any contact between the surfaces of the mask and the YBCO film is avoided. The parallel alignment of the mask relative to the prepatterned YBCO bridge is achieved via monitoring in an optical microscope with the help of marker holes in the Si membrane. Three different masks are used. For the main results, a square array of about 670×270 holes with diameters $D = (180 \pm 5)$ nm and a $d = (302 \pm 2)$ nm lattice constant is used, covering the entire YBCO bridge. Additional samples are irradiated through masks with the same hole diameters, but with 500-nm and 1-μm lattice constants, respectively. MIBS provides a 1:1 projection of the hole pattern inscribed in the mask since the ion beam can only reach the YBCO sample through the mask holes. The ion irradiation produces columnar defect-rich regions (CDs) in the sample [24]. All other parts of the sample, as well as the electrical contacts, are protected from irradiation. The second bridge on the substrate is not irradiated and serves as a reference.

The irradiations are performed with a fluence of 3×10^{15} cm^{-2} in a commercial ion implanter (High Voltage Engineering Europa B.V.) with rapid lateral beam scanning and dose monitoring by Faraday cups [24]. Beam current is kept small and the sample stage is cooled to avoid heating of the YBCO film above room temperature that might result in a loss of oxygen. The beam direction is parallel to the sample's *c*-axis direction. Figure 1(b) shows the resulting contrast pattern of the columnar defect array (CDA) at the surface of the YBCO film in a scanning-electron-microscopy picture. Note that the dark areas do not represent holes in the sample, but rather the different escape rate of secondary electrons from the irradiated material [25]. MIBS leads to a reduction of the critical temperature depending on the width of unirradiated channels between the CDs, resulting in $T_c \sim 47$ K ($d = 302$ nm), $T_c \sim 80$ K ($d = 500$ nm), and $T_c \sim 85$ K ($d = 1$ μm), respectively. Similar behavior was observed in other studies of CDAs that are produced by masked ion irradiation [11].

Somewhat different procedures for the patterning of HTSC films by ion irradiation have been reported by several groups. They have in common that the mask is directly deposited onto the sample's surface. Either photoresist is used as the ion-blocking material, with etched holes defined by optical [26], *e*-beam [11,13,15,16], or focused-ion-beam lithography [27], or a deposited metal layer that is patterned by ion-beam milling [28–30]. By contrast, current MIBS technology provides many advantages over other methods used for the nanopatterning of HTSCs: (1) The desired pattern is fabricated in a *single-step* process, directly resulting in the as-required modification of specific portions of the material. The extent of this change can be controlled by the ion fluence, leading to superconducting (with reduced T_c), normal conducting, or even insulating properties. (2) The method avoids any contact with the sample surface and does not require chemical treatment or etching, thus preventing possible surface damage. (3) It is a time-efficient parallel method applicable to large areas, and the mask can be reused many times, allowing for scalability in industrial manufacturing. (4) The surface remains essentially flat, which permits the preparation of multilayer structures and avoids deterioration of the film by an out-diffusion of oxygen through open side faces.

Magnetoresistance and critical current are measured in a closed-cycle refrigerator, with temperature control by a Cernox resistor [31]. The magnetic field, supplied by an electromagnet and oriented perpendicular to the sample surface, is monitored by a calibrated Hall probe with an accuracy of ± 1 mT. The critical current $I_c(B)$ is measured with two different procedures. To ensure that the vortices can arrange themselves in equilibrium positions throughout the sample, the YBCO film is field cooled (FC) from 100 K to the final measurement temperature. After a delay of 5 min to achieve thermal equilibrium, an exponential current ramp is executed until the voltage criterion of 100 nV, corresponding to 10 μV/cm, is reached. Subsequently, the temperature is raised again to 100 K, the magnetic field incrementally

increases or decreases, and the process repeats. Alternatively, the sample is cooled, with the magnetic field set to zero within the accuracy ± 1 mT of our gaussmeter [zero-field cooled (ZFC)] and the data is collected at the target temperature by ramping the magnetic field without warming up the sample. Corresponding protocols are used to measure the magnetoresistance $R(B)$.

III. RESULTS

The commensurate arrangement of vortices within a periodic lattice of pinning regions is commonly demonstrated by "vortex-matching" effects. For a square array of pins the (first) matching field is

$$B_m = \frac{\phi_0}{d^2}, \tag{1}$$

where ϕ_0 is the flux quantum. In principle, vortex matching can also occur at fields nB_m, with n being any rational number. For convenience, we will use $n = 0$ to denote the absence of vortices. The various arrangements of vortices with respect to the defect lattice for integer and fractional values of n have been visualized by Lorentz microscopy in a superconducting Nb film [3].

While vortex-matching effects in metallic superconductors have been investigated thoroughly with typically micrometer-sized antidot structures [1–3,5,9,32], few experiments have been reported for HTSCs. Peaks of the critical current [4,14] or minima in the magnetoresistance at nB_m [7,8,11,13,14] have been observed. Also, vortex ratchet and rectification effects have been reported in YBCO [18,20], as well as geometric frustration effects in nonuniform pinning arrays [15,16].

In Fig. 2, two different experimental tests for vortex-matching effects in the FC case are demonstrated. The critical current $I_c(B)$ at a temperature $T = 34.3$ K, corresponding to a reduced temperature $t = T/T_c = 0.73$, probes the static situation, where vortices are pinned, and the magnetoresistance $R(B)$ at $T = 36.0$ K ($t = 0.77$), the dynamic case where vortices move. The distinct maxima in $I_c(B)$ and the minima of $R(B)$ are positioned exactly at multiples of the matching field according to Eq. (1), where a commensurate relation exists between the vortex lattice and the CDA defined by the geometrical parameters of the stencil mask. Calculations in the framework of nonlinear Ginzburg-Landau theory predict a similar behavior of $I_c(B)$ for equilibrium vortex arrangements [33]. Careful inspection reveals signatures of vortex matching at $n = \frac{1}{2}$ and $n = \frac{3}{2}$, too. Naturally, with the absence of an external magnetic field, I_c attains a maximum and R a minimum.

The characteristic peaks and minima become less significant if the lattice spacing of the CDA is increased. In the $d = 500$ nm sample, they are still quite visible, whereas they are almost washed out in the $d = 1$ μm sample. This observation is in line with previous reports, where weak cusps in $I_c(B)$ were identified in a YBCO film perforated with a square array of holes [4] with $d = 1$ μm and in a $Bi_2Sr_2CaCu_2O_8$ (BSCCO) ribbon with $d = 0.5$ μm [8]. Conversely, in a YBCO film with $d = 120$ nm, a significant peak of $I_c(B)$ at B_m was seen [11]. We attribute the pronounced matching effects in our sample to the fact that the lattice constant of the CDA is comparable to the typical intrinsic defect spacing in epitaxial YBCO films.

A strikingly different picture arises in the ZFC experiments. Figure 3 presents $I_c(B)$ of the patterned YBCO

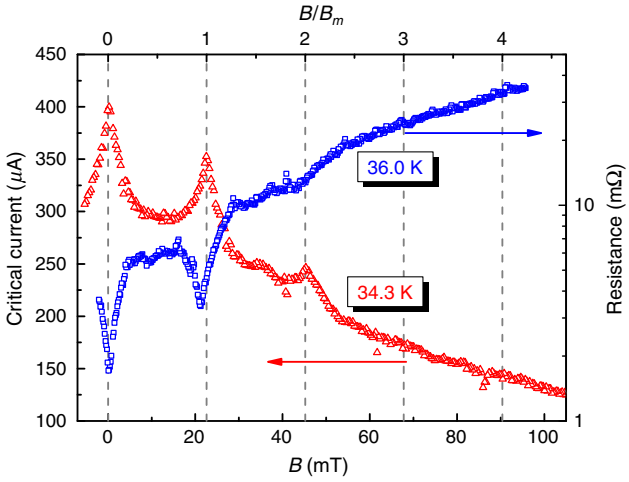

FIG. 2. Critical current and magnetoresistance as a function of the applied magnetic field B after field cooling the sample from $T = 100$ K for every data point. The upper horizontal axis is scaled to multiples of the matching field $B_m = 22.6$ mT.

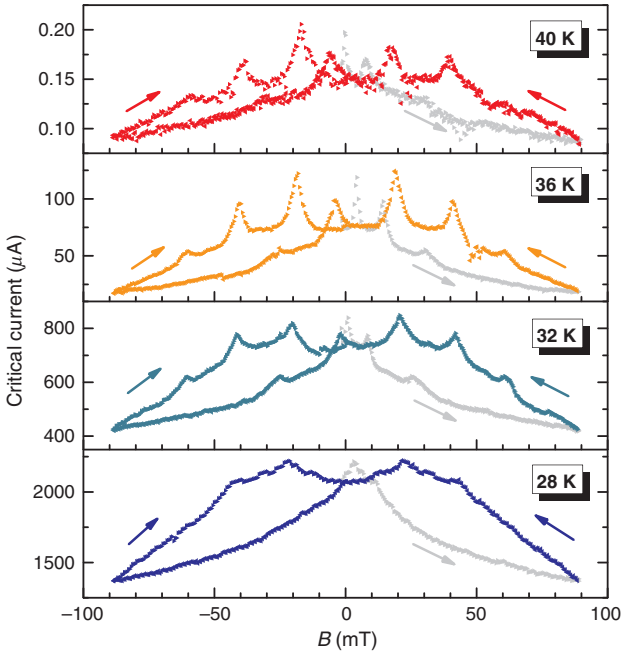

FIG. 3. Hysteretic behavior of the critical current after zero-field cooling at the respective temperature and ramping the applied magnetic field B through a full cycle. Gray symbols denote the virgin curve.

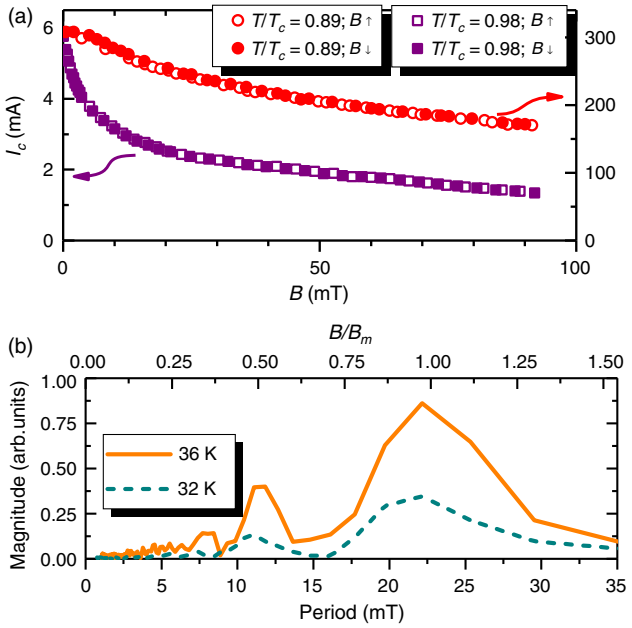

FIG. 4. (a) Critical current of the unirradiated reference bridge after ZFC in increasing (open symbols) and decreasing (solid symbols) magnetic field at $t = 0.89$ (circles) and $t = 0.98$ (squares), respectively. (b) Periodic components in the down-ramped branches from Fig. 3 determined via Fourier transform.

film for various temperatures after cooling from $T = 100$ K and then cycling the magnetic field. The gray branches represent the virgin curves and the bright-colored ones the decreasing-field ramp, and the light-colored branch returns to $B = 0$. We emphasize that a complementary procedure—in

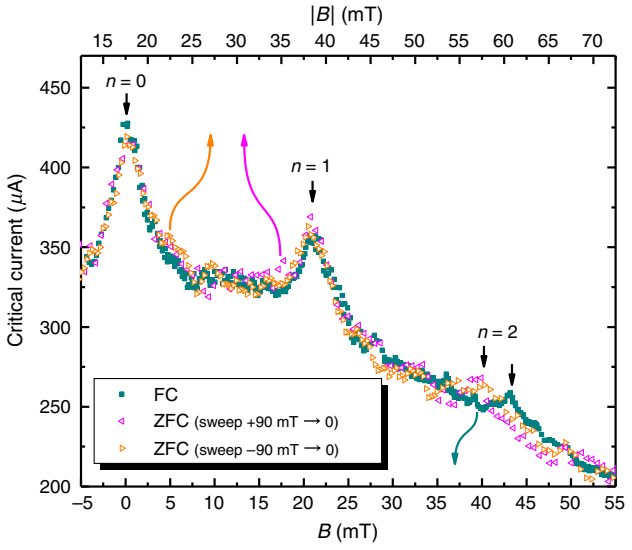

FIG. 5. Comparison of the shape of the matching peaks in zero-field cooled (ZFC) and field-cooled (FC) experiments at 35 K. The ZFC data are taken from the two branches of the hysteresis loop when the magnetic field is reduced. The displacement of the upper scale (the ZFC data) reflects the shift of the peaks due to the irreversible behavior.

which the sample is first cooled below T_c in a field of 90 mT and the magnetic field is then reduced—leads to the same curve as the ramped-down branch of the ZFC experiment in Fig. 3. All curves display a strong hysteresis during these cycles, in sharp contrast to most of the other related experiments, which did not report hysteretic effects of electrical-transport properties [7,8,10,11,13,15–17]. Only a tiny hysteresis of the critical current was reported in perforated Sn [1,5] and YBCO films [4] with a 1-μm interhole distance. Figure 4(a) demonstrates that irreversible effects are also absent in our unirradiated reference bridge.

While the peaks in the virgin curves seem to appear at irregular positions that cannot be correlated to matching fields, the decreasing-field data look very similar to the FC data in Fig. 2 but shifted by a magnetic field $B_{\text{shift}} = (19 \pm 2)$ mT. Thus, the field-ramped curves reveal the highest I_c at nonzero field. In addition, the distance between the n and $n+1$ peaks in I_c corresponds to B_m at all temperatures, despite a large variation of critical current and hysteresis area of the curves. Remarkably, even B_{shift} varies only slightly with temperature and the peaks can be observed over a wide temperature range $0.60 < t < 0.85$.

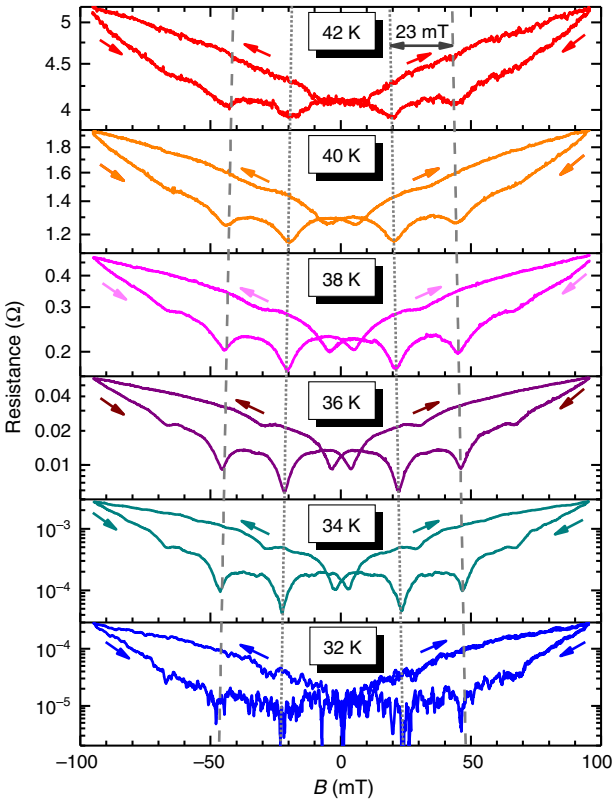

FIG. 6. Hysteretic behavior of the resistance after zero-field cooling at the respective temperature and ramping the applied magnetic field B through full cycles. The second cycle is shown to demonstrate the symmetry of the hysteresis and to exclude the virgin curve. The dotted lines represent the resistance minima corresponding to the $B = 0$ state, and the dashed lines those attributed to the first matching field.

This periodicity is better demonstrated by Fourier transforms of the down-ramped curves that reveal pronounced maxima at $B/B_m = n = 1$ and smaller peaks at $n = \frac{1}{2}$; see Fig. 4(b). A direct comparison of the FC and ZFC data collected in subsequent runs at the same temperature is presented in Fig. 5. As might be anticipated, the branches swept down from both polarities of the magnetic field are nearly identical. Intriguingly, however, the FC data also match almost perfectly, aside from a small offset of the $n = 2$ peak. These almost identical peak values and shapes indicate that the I_c peaks in both the FC and ZFC experiments must be caused by similar domains in which vortices are commensurate with the CDA.

An equivalent hysteresis with the same displacement B_{shift} of the matching peaks can be observed in the magnetoresistance measurements presented in Fig. 6. The temperature region where the hysteretic effects can be clearly observed extends close to T_c and into a regime of finite resistance and partial depinning of vortices. Another finding resulting from comparing the ZFC $I_c(B)$ and $R(B)$ measurements is that B_{shift} is independent of the time scale of the measurements. Collecting the magnetoresistance data for a full cycle takes about 24 h, whereas the sweep for the I_c measurement takes 2–4 days. Thus, the hysteretic effect is very robust over long time scales.

IV. DISCUSSION

At this time, it is useful to recall the particular geometry of our thin-film samples and relate them to superconducting parameters. The sample's thickness t_z is on the order of the zero-temperature in-plane London penetration depth $\lambda_{ab}(0) \sim 220$ nm in YBCO [34], the length and width are $l > w \gg \lambda_{ab}$. Hence, only marginal curvature of the vortices and their alignment parallel to the crystallographic c axis is expected for $B \parallel c$ in our experiments. However, strong demagnetization effects will be present and the critical state will deviate significantly from a simple Bean-model picture [35]. The diameter D of the defect columns and their lattice constant are also comparable to $\lambda_{ab}(0)$. The zero-temperature in-plane Ginzburg-Landau coherence length $\xi_{ab}(0) \sim 1.4\ \mathrm{nm} \ll D$ [36], thus allowing the accommodation of multiple fluxons in a CD [37].

An irreversible behavior of $I_c(B)$ (without vortex-matching effects) has been observed in granular YBCO and interpreted by a critical state together with trapped flux in the intergrain voids [38]. The related hysteretic behavior of the microwave surface resistance has been explained by a two-level critical-state model, presuming a local flux-density gradient within the grains that is different from the macroscopic one of the entire sample [39]. Remarkably strong flux gradients have been reported in BSCCO crystals within an area that is patterned with a blind hole array, but not in the neighboring pristine parts of the crystal [12]. Recently, a hysteretic behavior of the Josephson supercurrent in coplanar Al-graphene-Al junctions upon cycling the magnetic field was reported [40].

Geometric effects on the critical state of thin homogeneous superconducting strips, similar to the shape of our samples, have been evaluated by Brandt and Indenbom [35]. They calculated the current density and the magnetic field when both a perpendicular magnetic field and a transport current are applied together. The current density reaches its critical value j_c at one edge of the sample, falling off rapidly towards the center of the sample but remaining finite in the entire superconductor. The magnetic field exhibits a curved profile with a larger gradient near the sample's edge. Although these findings seem to complicate further considerations, they nevertheless prove that the critical state in our thin samples can be qualitative interpreted within the common critical-state models.

A possible scenario for the unconventional hysteretic shift of the matching peaks in our samples could be the trapping of a remanent field within the superconducting YBCO film due to the large intrinsic pinning of interstitial vortices that adds to the effects of vortex matching in the CDA. In fact, local scanning-Hall-probe measurements in perforated YBCO films revealed a hysteresis of magnetization between the holes [6]. However, a comparison of our samples with different d's demonstrates that wider lattices lead to a reduction of the hysteresis area and of B_{shift}, from $B_{\mathrm{shift}} \sim 19$ mT ($d = 302$ nm) to 2.5 mT ($d = 500$ nm) and 0.2 mT ($d = 1\ \mu$m) at $t = 0.98$. In the unpatterned reference YBCO bridge, no hysteresis is observed, as demonstrated in Fig. 4(a). Hence, the appearance of hysteresis appears to be connected with a sufficiently dense CDA and not with pinning of interstitial vortices in the superconducting material between the CDs.

In fact, in our system, two different vortex-pinning mechanisms are operative. On the one hand, fluxons are anchored by the normal cores of the CDs, and this pinning potential prevents them for entering the superconducting material between the CDs. Eventually, they can hop from one CD to a neighboring one [41]. On the other hand, interstitial vortices are pinned by intrinsic defects in the unirradiated parts of the sample. The peaks in I_c then arise from the fact that a larger number of fluxons is trapped in the CDs, and, conversely, the number of interstitial vortices is smaller. In fact, numerical simulations by Reichhardt *et al.* [42] predicted a complex dynamical behavior of moving vortices, including their one-dimensional channeling between periodic pinning arrays. The interplay between these two different pinning mechanisms was also addressed by Avci *et al.* [8] for perforated BSCCO films and by Trastoy *et al.* [13] for ion-beam patterned YBCO. However, neither study reported hysteretic transport properties.

To understand the irreversible behavior observed in our ZFC experiments, we propose that the magnetic-field gradient inside our sample is mainly established by the strong trapping of fluxons in the CDA, whereas the onset of

channeling of interstitial vortices limits the critical current to its rather low value. Thus, unlike in the Bean critical-state model for homogeneous superconductors, increasing the current up to I_c does not propagate the magnetic flux towards the sample's center. A much higher Lorentz force would be needed to unpin the fluxons locked at the CDA. The critical current is determined only by the interstitial vortices in a small zone at the sample's edge and is independent of the flux profile within the sample. In fact, Fig. 5 reveals that the size and the shape of the peaks are almost identical in FC and ZFC measurements and, thus, confirms that I_c must be dominated by similar mechanisms despite of different flux profiles.

Now, the strikingly robust distance between the matching peaks and minima, respectively, in ZFC measurements needs to be addressed. We presume that the critical state splits into uniform domains, in which every CD is populated by the same number of fluxons n, and neighboring regions by $n \pm 1$. Indeed, a terraced critical state was proposed for vortex-pinning lattices by Cooley and Grishin [43], where in circumferential regions of the sample the pinning centers are occupied by multivortices, with the nucleation of new terraces upon raising the magnetic field. However, their model is based on a thin superconducting slab in a parallel magnetic field without demagnetization effects. Although demagnetization would change the profile of magnetic induction to a more singular behavior near the edges of our samples, this effect is softened by a "smearing" to the order of the film thickness t_z [35]. Thus, a quantitative comparison of the terrace model's predictions with our experiments is not possible, but intriguing parallels on a qualitative level are obvious and are discussed below.

A key prediction of the terrace model is the periodicity of physical properties with the matching field when the magnetic field is ramped. Such periodicities were reported for the pinning force in NbTi composite wires [44] and the magnetization of Pb/Ge multilayers with a square lattice of submicron holes [2]. Another important feature of the terraced critical state is that the sample's magnetization is uniform within such a domain and has a strong gradient between neighboring terraces. The current in the sample stratifies into streamlines along the terrace edges but vanishes within a terrace [43].

For an estimate of the situation in our sample, we recall that matching effects are best seen in the down ramps of ZFC cycled fields, with the additional observation that $I_c(B)$ curves are the same when the sample is initially FC at 90 mT and data is then taken during the down ramp. Thus, we can conclude that, at 90 mT, the sample is field saturated in both experiments. Upon down sweep, a field gradient builds up, eventually leading to $B = B_m$ at the sample's edges and $B \lesssim 90\ \mathrm{mT} \sim 4B_m$ in its center. If we assume a terraced critical state with integer fillings of nB_m, it follows that about four terraces $n = 1, \ldots, 4$ can be present at the $n = 1$ peaks in Fig. 3. The width of a terrace roughly scales with n and is connected to λ_{ab} [43]. The width of the $n = 1$ terrace, thus, should be on the order of $w_{t1} \sim (w/2)/\sum_{n=1}^{4} n = 3\ \mu\mathrm{m} \sim 10d$ and should be slightly temperature dependent. However, owing to demagnetization effects, the terrace located at the sample's edge is probably somewhat smaller.

In an ideal terraced critical state every current streamline should be confined to a single unirradiated channel between two adjacent rows of CDs at the terrace edge with width $w_s = d - D \sim 120$ nm. Since the vorticity between such neighboring CDs changes by $\pm\phi_0$, the local current density in a channel would be $j_s = \phi_0/(\mu_0 d^2 w_s) \sim 15\ \mathrm{MA/cm^2}$. Our YBCO films have a $j_c(t = 0.77) \sim 7.2\ \mathrm{MA/cm^2} \sim j_s/2$ and $j_c(t = 0.85) \sim 3.8\ \mathrm{MA/cm^2} \sim j_s/4$, which indicates that the width of a current-carrying streamline will extend to at least $2d$ ($4d$) for the 36 K (40 K) data in Fig. 3. Within such streamlines, which encompass several rows of CDs, an incommensurate vortex placement is expected.

Our estimates can be compared to a two-dimensional dynamic simulation of vortex arrangements in a critical state with periodic arrays of pinning sites by Reichhardt *et al.* [45]. They found that, upon increasing the magnetic field from zero, a commensurate vortex lattice appears at the edge of the sample that persists for a finite range of the external magnetic field around the first matching peak. Upon further increasing B, the commensurate terrace is pushed inside the sample and the edge-region disorders before forming the next commensurable plateau. Remarkably, at higher matching fields, no terraces are found, but rather stripes and islands of a constant B, surrounded by current-carrying strings. Also, scanning-Hall-probe measurements in a perforated Pb thin film indicate a terraced critical state with increasing disorder at higher fields [9].

We propose a similar situation in our experiments. Since only matching peaks with $n \leq 2$ are visible, we conclude that the critical state in our sample features commensurate stripes near the sample's edge that are separated by more disordered current-carrying streamlines, and that the terraced critical state deteriorates at a higher n. In the framework of such a model, the peaks in I_c appear when a fully developed terrace occupies the edge of the sample and, hence, only a few interstitial vortices are available to be moved by the applied current. Upon increasing or decreasing the field, a disordered state with a higher density of interstitial vortices appears, reducing I_c, until the next terrace is formed. In addition, demagnetization effects are less important, allowing for wider commensurate domains, after the field was ramped down and the external magnetic field can partially penetrate the interior of the sample.

The observed matching effects are remarkably robust over the experimentally accessible temperature range. The hysteretic shift of the peaks and minima, respectively, B_{shift} changes only a little with T, $B_{\mathrm{shift}}(32\ \mathrm{K})/B_{\mathrm{shift}}(42\ \mathrm{K}) \sim 1.2$, less than $\lambda_{ab}(42\ \mathrm{K})/\lambda_{ab}(32\ \mathrm{K}) \sim 1.5$, and is therefore considered a nonrelevant effect. Obviously, the matching effects

disappear at high temperatures, where pinning at the CDA becomes negligible. More interesting is the behavior at low temperatures. Here, two effects can be considered. First, the intrinsic pinning becomes strong and interstitial vortices are immobilized, straightening out the matching peaks. Second, the self-field of I_c at 28 K reaches $B_{\rm sf}^{\rm max} = \mu_0 I_c/t_z \sim 13$ mT $\sim B_m/2$ and can displace or erode the terraces.

The strict periodicity of the I_c peaks in the FC experiment (Fig. 2) is evident from the matching condition of Eq. (1) but is not so straightforward to understand in the ZFC magnetic-field cycled experiments (Figs. 3 and 6), where it is observed over a wide temperature range. In fact, the terraced critical-state model [43] predicts the formation of a new terrace with $n+1$ fluxon occupation per CD at the sample's edge when the field is increased by $\Delta B_{n,n+1} = B_m$ and, conversely, a corresponding depletion of terraces when the field is reduced. However, it follows from Eq. (1) that one flux quantum per CD must be added or removed over the *entire* sample area. The virgin curves in Fig. 3 demonstrate that this is indeed not the case when magnetic flux enters into the sample from the edge after ZFC and the CDs in the inner parts of the sample are not yet populated by fluxons; thus, $\Delta B_{n,n+1} < B_m$ ($n = 0$ or 1). Conversely, after field saturating the sample and then ramping down, a monotonically decreasing critical-flux profile establishes from the center to the edge of the sample, so that by extracting fluxons from the outermost terrace, a redistribution (and extraction) in the entire sample takes place. This scenario also holds when terraces with a higher n inside the sample are partially disordered or do not exist at all. A similar periodicity and temperature independence has been also observed in magnetization measurements in perforated Pb/Ge multilayers [2].

The observed hystereses in I_c (Fig. 3) and R (Fig. 6) have their origin in the different magnetization profiles during up and down ramps, respectively, which result in different occupation numbers of the outermost terrace at the sample's edge at the same external magnetic field. Since the current will concentrate at the sample's edge, the outermost terrace determines the transport properties and gives rise to matching peaks shifted away from their equilibrium positions.

To summarize, a terraced critical state or a similar commensurate vortex domain structure at the sample's edge provides a plausible scenario for our observations, particularly for the equidistance of the matching peaks, where I_c is determined by the vortex arrangement at the sample's fringes. Evidently, for an in-depth understanding of these effects, additional theoretical efforts and simulations are required.

V. CONCLUSIONS

In this paper, we demonstrate the fabrication of submicrometer CDAs in thin YBCO films with an alternative, noncontact, single-step ion irradiation technique. The method features a 1:1 reproduction of a periodic structure from a perforated Si stencil mask and has the potential to be further developed into an ion-projection technique with ion-optical reduction [46]. Strong commensurability effects are observed between flux quanta and the CDA in both equilibrium and nonequilibrium fluxon arrangements. They manifest themselves in pronounced maxima of the critical current and minima of the magnetoresistance. In ZFC and magnetic-field ramped data, the matching pattern is displaced, but the equidistance between the matching peaks is conserved, which could be an indication of an unconventional—probably terraced—critical state that calls for further investigation. Finally, our results demonstrate an ordered out-of-equilibrium arrangement of flux quanta with long-term stability in a superconductor and pave the way for the envisaged fluxonic devices.

ACKNOWLEDGMENTS

We appreciate the help of Klaus Haselgrübler with the ion implanter. M. D. acknowledges support from the Erasmus Mundus program. This work was supported by the COST Action MP-1201.

[1] A. N. Lykov, Pinning in superconducting films with triangular lattice of holes, Solid State Commun. **86**, 531 (1993).
[2] M. Baert, V. V. Metlushko, R. Jonckheere, V. V. Moshchalkov, and Y. Bruynseraede, Composite Flux-Line Lattices Stabilized in Superconducting Films by a Regular Array of Artificial Defects, Phys. Rev. Lett. **74**, 3269 (1995).
[3] K. Harada, O. Kamimura, H. Kasai, T. Matsuda, A. Tonomura, and V. V. Moshchalkov, Direct observation of vortex dynamics in superconducting films with regular arrays of defects, Science **274**, 1167 (1996).
[4] A. Castellanos, R. Wördenweber, G. Ockenfuss, A. v. d. Hart, and K. Keck, Preparation of regular arrays of antidots in $YBa_2Cu_3O_7$ thin films and observation of vortex lattice matching effects, Appl. Phys. Lett. **71**, 962 (1997).
[5] A. N. Lykov, Unusual commensurability effect in superconducting Sn films with triangular lattice of microholes, J. Low Temp. Phys. **164**, 61 (2011).
[6] A. Crisan, A. Pross, D. Cole, S. J. Bending, R. Wördenweber, P. Lahl, and E. H. Brandt, Anisotropic vortex channeling in $YBa_2Cu_3O_{7-\delta}$ thin films with ordered antidot arrays, Phys. Rev. B **71**, 144504 (2005).
[7] S. Ooi, T. Mochiku, S. Yu, E. S. Sadki, and K. Hirata, Matching effect of vortex lattice in $Bi_2Sr_2CaCu_2O_{8+y}$ with artificial periodic defects, Physica (Amsterdam) **426C–431C**, 113 (2005).
[8] S. Avci, Z. L. Xiao, J. Hua, A. Imre, R. Divan, J. Pearson, U. Welp, W. K. Kwok, and G. W. Crabtree, Matching effect and dynamic phases of vortex matter in $Bi_2Sr_2CaCu_2O_8$ nanoribbon with a periodic array of holes, Appl. Phys. Lett. **97**, 042511 (2010).
[9] A. V. Silhanek, J. Gutierrez, R. B. G. Kramer, G. W. Ataklti, J. Van de Vondel, V. V. Moshchalkov, and A. Sanchez, Microscopic picture of the critical state in a superconductor

with a periodic array of antidots, Phys. Rev. B **83**, 024509 (2011).

[10] I. Sochnikov, I. Bozovic, A. Shaulov, and Y. Yeshurun, Uncorrelated behavior of fluxoids in superconducting double networks, Phys. Rev. B **84**, 094530 (2011).

[11] I. Swiecicki, C. Ulysse, T. Wolf, R. Bernard, N. Bergeal, J. Briatico, G. Faini, J. Lesueur, and J. E. Villegas, Strong field-matching effects in superconducting $YBa_2Cu_3O_{7-\delta}$ films with vortex energy landscapes engineered via masked ion irradiation, Phys. Rev. B **85**, 224502 (2012).

[12] G. Shaw, B. Bag, S. S. Banerjee, H. Suderow, and T. Tamegai, Generating strong magnetic flux shielding regions in a single crystal of $Bi_2Sr_2CaCu_2O_8$ using a blind hole array, Supercond. Sci. Technol. **25**, 095016 (2012).

[13] J. Trastoy, V. Rouco, C. Ulysse, R. Bernard, A. Palau, T. Puig, G. Faini, J. Lesueur, J. Briatico, and J. E. Villegas, Unusual magneto-transport of $YBa_2Cu_3O_{7-\delta}$ films due to the interplay of anisotropy, random disorder and nanoscale periodic pinning, New J. Phys. **15**, 103022 (2013).

[14] L. T. Haag, G. Zechner, W. Lang, M. Dosmailov, M. A. Bodea, and J. D. Pedarnig, Strong vortex matching effects in YBCO films with periodic modulations of the superconducting order parameter fabricated by masked ion irradiation, Physica (Amsterdam) **503C**, 75 (2014).

[15] J. Trastoy, M. Malnou, C. Ulysse, R. Bernard, N. Bergeal, G. Faini, J. Lesueur, J. Briatico, and J. E. Villegas, Freezing and thawing of artificial ice by thermal switching of geometric frustration in magnetic flux lattices, Nat. Nanotechnol. **9**, 710 (2014).

[16] J. Trastoy, C. Ulysse, R. Bernard, M. Malnou, N. Bergeal, J. Lesueur, J. Briatico, and J. E. Villegas, Tunable Flux-Matching Effects in High-T_c Superconductors with Non-uniform Pinning Arrays, Phys. Rev. Applied **4**, 054003 (2015).

[17] N. Poccia, T. I. Baturina, F. Coneri, C. G. Molenaar, X. R. Wang, G. Bianconi, A. Brinkman, H. Hilgenkamp, A. A. Golubov, and V. M. Vinokur, Critical behavior at a dynamic vortex insulator-to-metal transition, Science **349**, 1202 (2015).

[18] R. Wördenweber, P. Dymashevski, and V. R. Misko, Guidance of vortices and the vortex ratchet effect in high-T_c superconducting thin films obtained by arrangement of antidots, Phys. Rev. B **69**, 184504 (2004).

[19] S. Ooi, S. Savel'ev, M. B. Gaifullin, T. Mochiku, K. Hirata, and F. Nori, Nonlinear Nanodevices Using Magnetic Flux Quanta, Phys. Rev. Lett. **99**, 207003 (2007).

[20] A. Palau, C. Monton, V. Rouco, X. Obradors, and T. Puig, Guided vortex motion in $YBa_2Cu_3O_7$ thin films with collective ratchet pinning potentials, Phys. Rev. B **85**, 012502 (2012).

[21] M. B. Hastings, C. J. Olson Reichhardt, and C. Reichhardt, Ratchet Cellular Automata, Phys. Rev. Lett. **90**, 247004 (2003).

[22] M. V. Milošević, G. R. Berdiyorov, and F. M. Peeters, Fluxonic cellular automata, Appl. Phys. Lett. **91**, 212501 (2007).

[23] B. Dam, J. M. Huijbregtse, F. C. Klaassen, R. C. F. van-der Geest, G. Doornbos, J. H. Rector, A. M. Testa, S. Freisem, J. C. Martinez, B. Stauble-Pumpin, and R. Griessen, Origin of high critical currents in $YBa_2Cu_3O_{7-\delta}$ superconducting thin films, Nature (London) **399**, 439 (1999).

[24] W. Lang, M. Dineva, M. Marksteiner, T. Enzenhofer, K. Siraj, M. Peruzzi, J. D. Pedarnig, D. Bäuerle, R. Korntner, E. Cekan, E. Platzgummer, and H. Loeschner, Ion-beam direct-structuring of high-temperature superconductors, Microelectron. Eng. **83**, 1495 (2006).

[25] J. D. Pedarnig, K. Siraj, M. A. Bodea, I. Puica, W. Lang, R. Kolarova, P. Bauer, K. Haselgrübler, C. Hasenfuss, I. Beinik, and C. Teichert, Surface planarization and masked ion-beam structuring of $YBa_2Cu_3O_7$ thin films, Thin Solid Films **518**, 7075 (2010).

[26] F. Kahlmann, A. Engelhardt, J. Schubert, W. Zander, Ch. Buchal, and J. Hollkott, Superconductor-normal-superconductor Josephson junctions fabricated by oxygen implantation into $YBa_2Cu_3O_{7-\delta}$, Appl. Phys. Lett. **73**, 2354 (1998).

[27] A. S. Katz, S. I. Woods, and R. C. Dynes, Transport properties of high-T_c planar Josephson junctions fabricated by nanolithography and ion implantation, J. Appl. Phys. **87**, 2978 (2000).

[28] D. J. Kang, G. Burnell, S. J. Lloyd, R. S. Speaks, N. H. Peng, C. Jeynes, R. Webb, J. H. Yun, S. H. Moon, B. Oh, E. J. Tarte, D. F. Moore, and M. G. Blamire, Realization and properties of $YBa_2Cu_3O_{7-\delta}$ Josephson junctions by metal masked ion damage technique, Appl. Phys. Lett. **80**, 814 (2002).

[29] M. G. Blamire, D. J. Kang, G. Burnell, N. H. Peng, R. Webb, C. Jeynes, J. H. Yun, S. H. Moon, and B. Oh, Masked ion damage and implantation for device fabrication, Vacuum **69**, 11 (2002).

[30] N. Bergeal, X. Grison, J. Lesueur, G. Faini, M. Aprili, and J. P. Contour, High-quality planar high-T_c Josephson junctions, Appl. Phys. Lett. **87**, 102502 (2005).

[31] G. Heine and W. Lang, Magnetoresistance of the new ceramic "Cernox" thermometer from 4.2 K to 300 K in magnetic fields up to 13 T, Cryogenics **38**, 377 (1998).

[32] V. V. Metlushko, M. Baert, R. Jonckheere, V. V. Moshchalkov, and Y. Bruynseraede, Matching effects in Pb/Ge multilayers with the lattice of submicron holes, Solid State Commun. **91**, 331 (1994).

[33] G. R. Berdiyorov, M. V. Milošević, and F. M. Peeters, Vortex configurations and critical parameters in superconducting thin films containing antidot arrays: Nonlinear Ginzburg-Landau theory, Phys. Rev. B **74**, 174512 (2006).

[34] J.-Y. Lee and T. R. Lemberger, Penetration depth $\lambda(T)$ of $YBa_2Cu_3O_{7-\delta}$ films determined from the kinetic inductance, Appl. Phys. Lett. **62**, 2419 (1993).

[35] E. H. Brandt and M. Indenbom, Type-II-superconductor strip with current in a perpendicular magnetic field, Phys. Rev. B **48**, 12893 (1993).

[36] W. Lang, Study of superconducting fluctuations in the high-temperature superconductor $YBa_2Cu_3O_7$ by magnetotransport measurements, Synth. Met. **71**, 1555 (1995).

[37] A. I. Buzdin, Multiple-quanta vortices at columnar defects, Phys. Rev. B **47**, 11416 (1993).

[38] J. E. Evetts and B. A. Glowacki, Relation of critical current irreversibility to trapped flux and microstructure in polycrystalline $YBa_2Cu_3O_7$, Cryogenics **28**, 641 (1988).

[39] L. Ji, M. S. Rzchowski, N. Anand, and M. Tinkham, Magnetic-field-dependent surface resistance and two-level critical-state model for granular superconductors, Phys. Rev. B **47**, 470 (1993).

[40] D. Massarotti, B. Jouault, V. Rouco, S. Charpentier, T. Bauch, A. Michon, A. De Candia, P. Lucignano, F. Lombardi, F. Tafuri, and A. Tagliacozzo, Incipient Berezinskii-Kosterlitz-Thouless transition in two-dimensional coplanar Josephson junctions, Phys. Rev. B **94**, 054525 (2016).

[41] M. P. Sørensen, N. F. Pedersen, and M. Ögren, The dynamics of magnetic vortices in type II superconductors with pinning sites studied by the time dependent Ginzburg-Landau model, Physica (Amsterdam) **533C**, 40 (2017).

[42] C. Reichhardt, C. J. Olson, and F. Nori, Nonequilibrium dynamic phases and plastic flow of driven vortex lattices in superconductors with periodic arrays of pinning sites, Phys. Rev. B **58**, 6534 (1998).

[43] L. D. Cooley and A. M. Grishin, Pinch Effect in Commensurate Vortex-Pin Lattices, Phys. Rev. Lett. **74**, 2788 (1995).

[44] L. D. Cooley, P. J. Lee, D. C. Larbalestier, and P. M. O'Larey, Periodic pin array at the fluxon lattice scale in a high-field superconducting wire, Appl. Phys. Lett. **64**, 1298 (1994).

[45] C. Reichhardt, J. Groth, C. J. Olson, S. B. Field, and F. Nori, Spatiotemporal dynamics and plastic flow of vortices in superconductors with periodic arrays of pinning sites, Phys. Rev. B **54**, 16108 (1996).

[46] S. Eder-Kapl, A. Steiger-Thirsfeld, M. Wellenzohn, A. Koeck, R. Hainberger, H. Loeschner, and E. Platzgummer, Ion multi-beam direct sputtering of Si imprint stamps and simulation of resulting structures, J. Micromech. Microeng. **22**, 055008 (2012).